

わずに形態観察により胚盤胞と判定した胚を移植した対照群では、18匹の受容雌マウスに合計175個の胚を移植した結果、7匹が分娩(38.9%)し、合計41匹の産子を得た(産子率:23.4%)。一方、測定群では16匹の受容雌マウスに合計170個の胚を移植した結果、12匹が分娩(分娩率:75.0%)、合計67匹の産子が得られ(産子率:39.4%)、対照群と比較して移植成績が有意に上昇した。

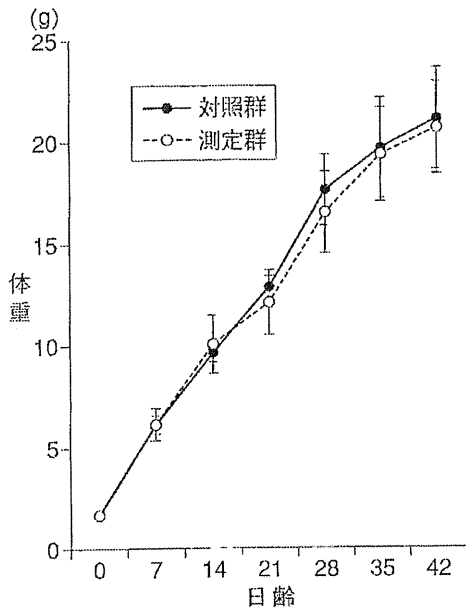


図2 体重成長曲線
生後0~42日の体重変化を示す。
(エラーバーは平均値±標準誤差)

4. 表現型解析

受精卵呼吸測定装置による胚品質評価の安全性を検証する目的で、胚移植試験で得られた産子の表現型解析を実施した。産子の生時体重の平均は、対照群で 1.55 ± 0.02 g, 測定群で 1.51 ± 0.04 g で有意差はなく、その後の体重増加にも有意差は認められなかった(図2)。また、Gバンド法による染色体検査(図3)や主要臓器(脳、肺、胃、腎臓、肝臓、膵臓、脾臓、心臓、大腿二頭筋、卵巣、精巣)の組織学的検査、血液生化学検査においても異常所見は認められなかった。また、行動解析(一般活動性・情動性・馴

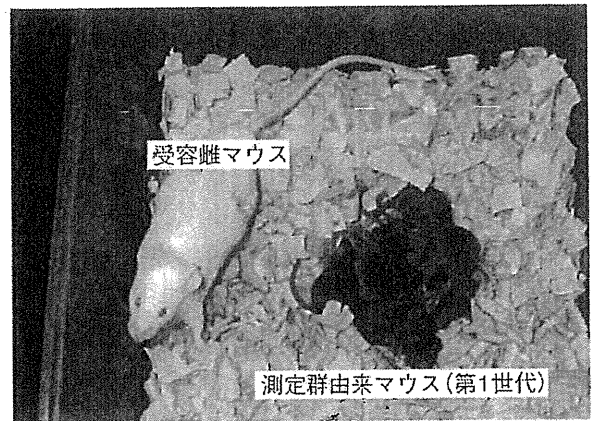


図4 測定群由来のマウス
性成熟後、5世代までの繁殖試験を実施したが、いずれの世代でも繁殖能力に異常はみられなかった。

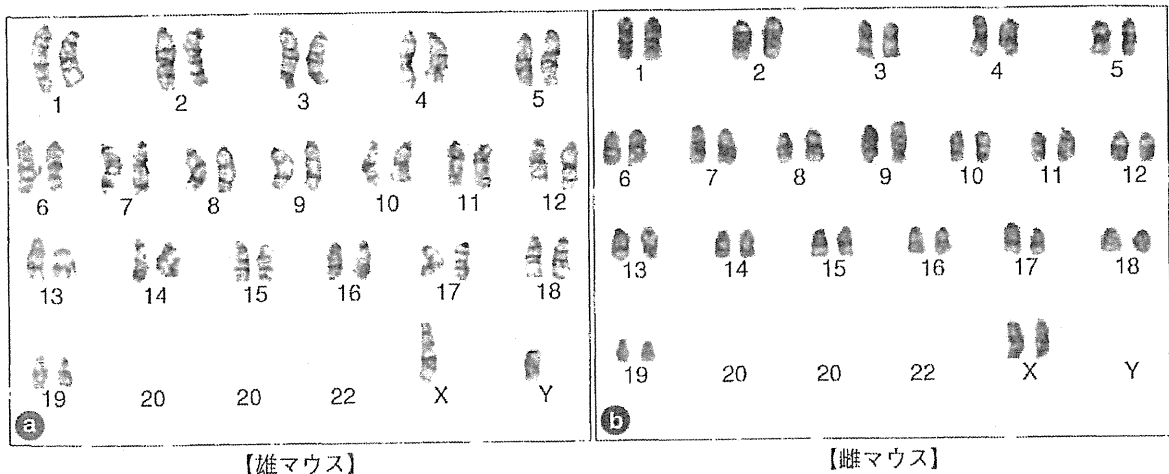


図3 染色体解析(Gバンド解析)
解析したマウス(30匹:雄12匹,雌18匹)すべてが $2n=40$ の正常な核型を有していた。

化の試験としてオープンフィールドテスト、運動能力・体力の試験としてオープンスペース水泳テスト、空間認知・学習能力・記憶力の試験として水迷路学習テストおよびプローブテスト)を実施したが、いずれのテストにおいても対照群と測定群のマウスで有意差は認められなかった。さらに、測定群の産子は性成熟後に繁殖試験を実施し、少なくとも5世代目までは正常な繁殖能力を有していることが確認された(図4)。

II. 考 察

近年の不妊治療件数の増加とともに多胎妊娠数も増加している。わが国では、生殖補助医療に伴って発生する多胎妊娠を減少させることが急務であるとし、2007年3月には日本生殖医学会が「多胎妊娠防止のための移植胚数ガイドライン」を、2008年4月には日本産科婦人科学会が「生殖補助医療における多胎妊娠防止に関する見解」を発表している。いずれの内容も、母体および胎児・新生児の健全なる福祉を保持する観点から、35歳以下の患者に対する胚移植においては、移植する胚の数を「原則1個」とすることが示されている。また、Velevaら⁵⁾は、36~39歳の患者に対しても単一胚移植を実施し、妊娠率、正常分娩率が複数胚(2個)移植の場合と比較して統計的有意差がないことを報告している。これらのことから、生殖補助医療における単一胚移植は、今後、幅広い年齢層の患者に対してますます重要になってくる可能性が考えられる。

単一胚移植における胚の評価に求められることは、できるだけ低侵襲に、再現性の高い方法で、移植に供する個々の胚の品質を正確に評価・選別することである。このことは妊娠率の向上だけではなく、流産・死産率の低下にもつながる。現在、生殖補助医療の臨床現場の多くは、Veck⁶⁾やGardnerら⁷⁾が提唱したヒト胚の品質評価法を採用している。これらの評価方法は、胚の割球数や形態を基準としており、現状

では、最も簡便で有効な方法である。しかしながら、最近、経時的な胚の観察研究などから、胚の品質を評価する上で形態を基準にするだけでは決して十分ではないことが指摘されている⁸⁾⁹⁾。また、形態的基準による判断だけでは、観察者の主観が影響する可能性が高く、検査結果の客観性に疑問が残る。

一方で、本研究で使用した受精卵呼吸測定装置は、個々の胚の酸素消費量を数値化できるため、客観的に胚の評価・選別が可能である。本研究では、妊娠4日目のマウスから得られた胚盤胞を①形態的基準のみで評価した胚(対照群)と②形態評価に加え呼吸活性を評価基準に評価した胚(測定群)に分けて移植した結果、測定群は対照群と比較して妊娠率、産子率が有意に上昇することが確認された。同様の結果は、ウシを用いた胚移植試験においても得られている³⁾¹⁰⁾。さらに本研究では、得られた産子の正常性についても様々な角度から検証し、呼吸活性を測定した胚を移植しても、その産子に異常はみられないことを確認した。従って、これらの結果から、胚の評価に呼吸活性の指標を加えることは、従来の形態的基準のみで評価する方法よりも有効な方法であり、胚やその後の個体発生への影響が少ない安全な方法であることが示唆された。

今回の結果はマウス胚を用いたものであり、ヒト胚における有効性、安全性については今後の課題である。しかしながら、この測定技術の注目すべき点は胚の酸素消費量(ミトコンドリア機能)を評価していることである。ミトコンドリアはすべての真核細胞に普遍的に存在している細胞内小器官である。従って、本研究で得られたマウスの結果をヒトへ直接外挿できる可能性は高いとわれわれは考えている。

おわりに

本研究では、マウスをモデル動物として、受精卵呼吸測定装置の有効性と安全性を検証した。その結果、呼吸活性を指標として胚の品質

を評価することで、移植成績の向上が認められた。さらに、得られた産子に異常所見はみられなかった。これらの結果から、電気化学的な胚の呼吸測定技術が、胚移植時における胚の品質評価法として有効かつ安全であることが示唆された。今後、ヒト胚における検証を十分に重ねるとともに、胚の呼吸活性と受胎（妊娠）との関係を詳しく調べることで、さらに安全性や精度を高めることができると考えている。近い将来、呼吸測定技術および装置が生殖補助医療における臨床応用へつながっていくことを期待している。

文 献

- 1) Shiku H, Shiraishi T, Ohya H, et al : Oxygen consumption of single bovine embryos probed by scanning electrochemical microscopy. *Anal Chem*, **73** : 3751-3758, 2001.
- 2) Shiku H, Shiraishi T, Aoyagi S, et al : Respiration activity of single bovine embryos entrapped in a cone-shaped microwell monitored by scanning electrochemical microscopy. *Anal Chim Acta*, **522** : 51-58, 2004.
- 3) Abe H, Shiku H, Yokoo M, et al : Evaluating the quality of individual embryos with a non-invasive and highly sensitive measurement of oxygen consumption by scanning electrochemical microscopy. *J Reprod Dev*, **52**(suppl): s55-s64, 2006.
- 4) Abe H : A non-invasive and sensitive method for measuring cellular respiration with a scanning electrochemical microscopy to evaluate embryo quality. *J Mamm Ova Res*, **24** : 70-78, 2007.
- 5) Veleva Z, Vilska S, Hydén-Granskog C, et al : Elective single embryo transfer in women aged 36-39 years. *Hum Reprod*, **21** : 2098-2102, 2006.
- 6) Veeck LL : Atlas of the human oocytes and early conceptus. Williams & Wilkins. **2**, 151-153, Baltimore, 1991.
- 7) Gardner DK, Lane M, Stevens J, et al : Blastocyst score affects implantation and pregnancy outcome : towards a single blastocyst transfer. *Fertil Steril*, **73** : 1155-1158, 2000.
- 8) Mio Y, Maeda K : Time-lapse cinematography of dynamic changes occurring during *in vitro* development of human embryos. *Am J Obstet Gynecol*, **660** : e1-5, 2008.
- 9) Okitsu O : Human embryo grading. *J Mamm Ova Res*, **25** : 90-97, 2008.
- 10) Moriyasu S, Hirayama H, Sawai K, et al : Relationship between the respiratory activity and the pregnancy rate of bisected bovine. *Reprod Fertil Dev*, **19** : 219, 2007.

選択的単一胚移植 (eSET) における移植胚選別 困難例に対する呼吸量測定の有用性

後藤香里 小池 恵 熊迫陽子 宇津宮隆史 阿部宏之

臨床 経験

選択的単一胚移植 (eSET) における移植胚選別困難例に対する呼吸量測定の有用性

後藤 香里* 小池 恵* 熊迫 陽子* 宇津宮隆史* 阿部 宏之**

eSET は最も発育能のある胚を見分け移植することが望まれる。移植胚選別において、Day 3 の形態評価に呼吸量評価を加えることで発育能のある胚が選別できるか検討した。Day 3 の分割別に呼吸量の違いによる胚盤胞到達率を調べたところ、形態評価のみで高率に胚盤胞へ到達する 8 分割を除いた 9 分割以上、7, 6 分割で呼吸量を測ることで胚盤胞到達胚の選別が可能となった。呼吸量が最も大きい胚を移植した場合、形態評価のみの移植と比較して、高い妊娠率と低い流産率が得られた。また呼吸量測定した胚移植で健常な出生を確認した。

はじめに

近年の妊娠率向上、多胎率の上昇に伴い体外受精の移植胚は 1 個とすることが求められている¹⁾。着床能のある 1 個の胚を見分け移植することが望まれるが、移植時に形態が等しく、選別困難である場合も少なくはない。妊娠率を低下させることなく多胎率、流産率を減少させるには、より着床しうる能力を持った 1 個の胚を選択することが不可欠である。現在、胚の評価は簡単で非侵襲的な方法である顕微鏡下での形態評価のみで行われている。しかし、形態評価は観察者の主観により判定結果に差が生じる可能性があるため、より客観的で精度が高く、安全な胚評価法の開発が望まれている。電気化学計測技術を基盤とする走査型電気化学顕微鏡は受精卵の呼吸活性を非侵襲的に測定することが

できる。

この細胞呼吸能測定による胚評価法を形態評価に加えることで、最も着床能のある 1 個の胚を見分けることが可能となるか検討した。呼吸量測定後、出産した症例についての出生結果も報告する。

1. 対象および方法

呼吸量測定装置と、測定の概略を示す (図 1)。方法は那須らの方法に順じた²⁾。

1. 検討 1: Day 3 (媒精後 3 日目) の分割数と呼吸量の関係

2006 年 7 月～2009 年 9 月に、Day 3-eSET (elective Single Embryo Transfer) 予定となり、移植時 Veeck の分類にてグレード 1 もしくは 2 である良好胚が 2 個以上存在し移植胚の選別が困難と思われる 307 症例 574 個の胚を対象とした。Day 3 に観察した分割数別に、胚呼吸量を調べ、胚盤胞到達率を調べた。測定後移植した胚は今回の検討から除いている。

2. 検討 2: eSET における検討

2007 年 3 月～2009 年 9 月に Veeck による形態評価がまったく等しい良好胚が 2 個以上存在

*Kaori GOTO, Megumi KOIKE, Yoko KUMASAKO, Takafumi UTSUNOMIYA
セント・ルカ産婦人科

**Hiroyuki ABE
山形大学大学院理工学研究科物質化学工学専攻
〒870-0947 大分県大分市津守富岡 5 組 (セント・ルカ産婦人科)

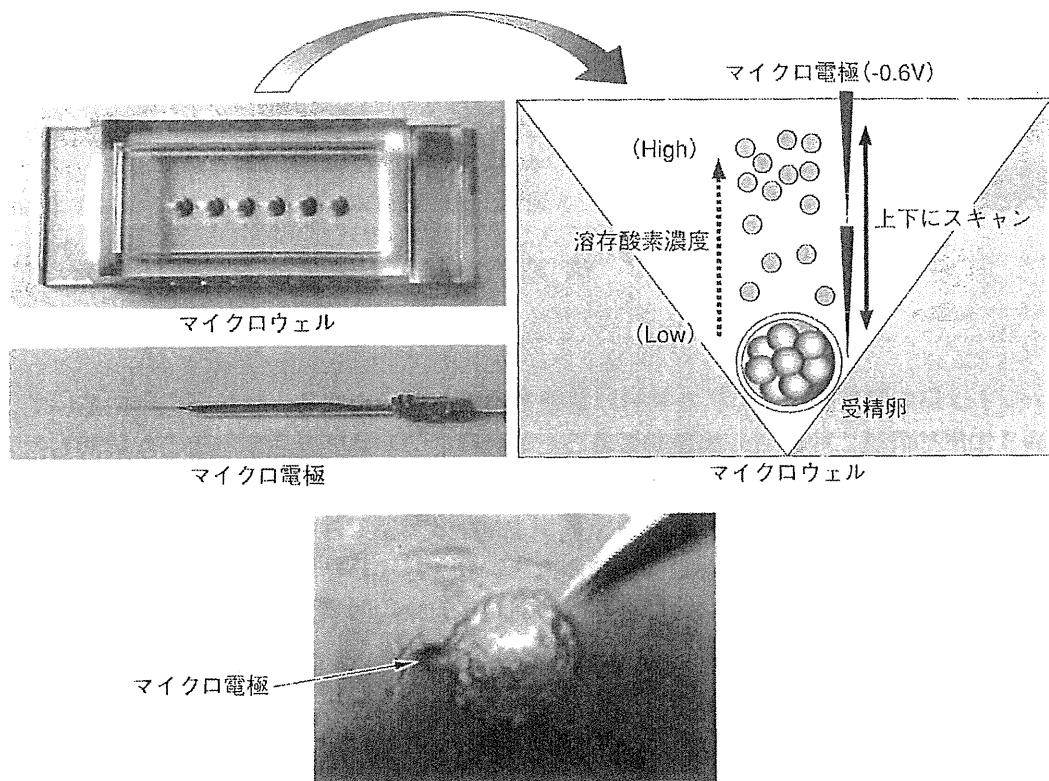


図1 呼吸量測定の概略

し、Day 3-eSET を行った症例 68 周期を対象とした。前方視的検討として Day 3 の形態がまったく同じ良好胚が 2 個以上存在した場合、移植胚の選択は無作為に呼吸量測定群と形態評価のみの群に振り分け、妊娠率、流産率、継続妊娠率を検討した。

3. 検討 3: 出生について

呼吸量評価が高く移植胚となり、出産に至った出生結果を形態評価のみで出産した場合と比較した。

II. 結 果

1. 検討 1

Day 3 で 9 割球以上に分割していた胚の胚盤胞到達率は呼吸量 $0.3 \times 10^{14} / \text{mols}^{-1}$ 未満で 46.2%, 0.3~0.4 未満で 81.8%, 0.4~0.5 未満は 66.7%, 0.5 以上で 65.5% と 0.3 未満と比較し 0.3~0.4 未満で胚盤胞到達率は高くなる結果を示した ($p < 0.05$)。8 分割胚では呼吸量の差に

よる発育の違いは認めなかった (77.1%, 70.2%, 76.7%, 83.3%) (図 2)。

7 分割胚ではどの群にも有意差は認めなかったが、呼吸量が大きくなるに従い胚盤胞到達率が高くなる傾向を示した (50.0%, 61.3%, 56.0%, 69.4%)。6 分割胚ではその傾向も顕著となり、呼吸量 0.3 未満と比べ、0.5 以上で胚盤胞到達率は有意に高くなる結果を認めた ($p < 0.05$) (29.4%, 38.2%, 50.0%, 57.1%) (図 3)。

2. 検討 2

形態評価がまったく等しい良好胚が 2 個以上ある移植胚選別困難例において、呼吸量測定群の妊娠率は 50.0%, 形態評価のみの群は 26.5% で呼吸量の大きい胚を移植することにより、高い妊娠率が得られた ($p < 0.05$) (図 4)。流産率は呼吸量評価を加えた群で 5.9%, 形態評価のみでは 22.2% と呼吸量評価を加えた群で低くなる傾向を示した。継続妊娠率は、従来の形態評価のみでは 20.6% であったのに対し、呼吸量評価を行うことで 47.1% にまで向上した ($p < 0.05$)。

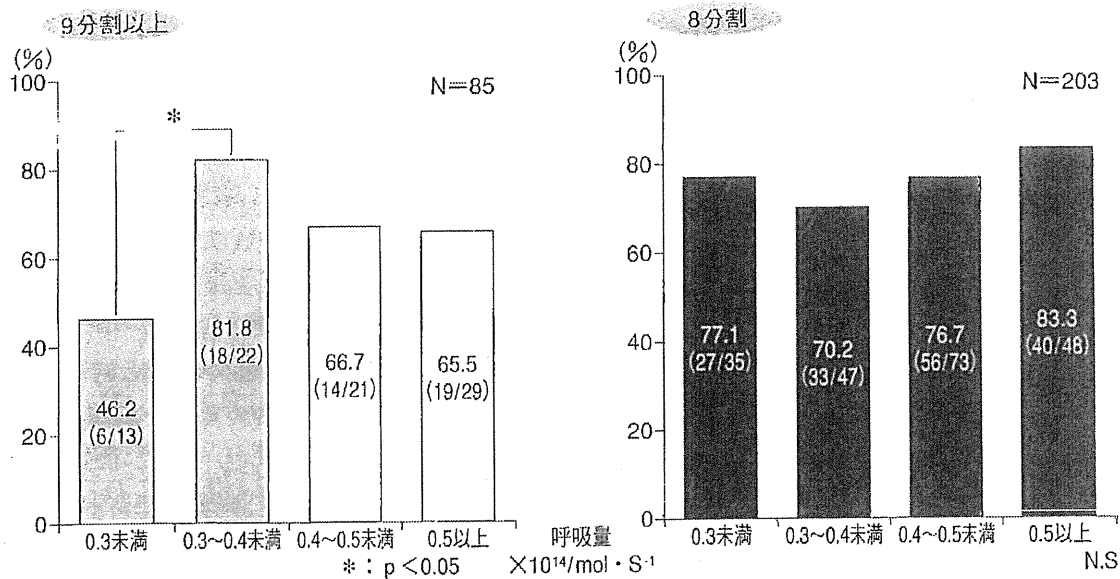


図2 分割数別にみた胚呼吸量と胚盤胞到達率

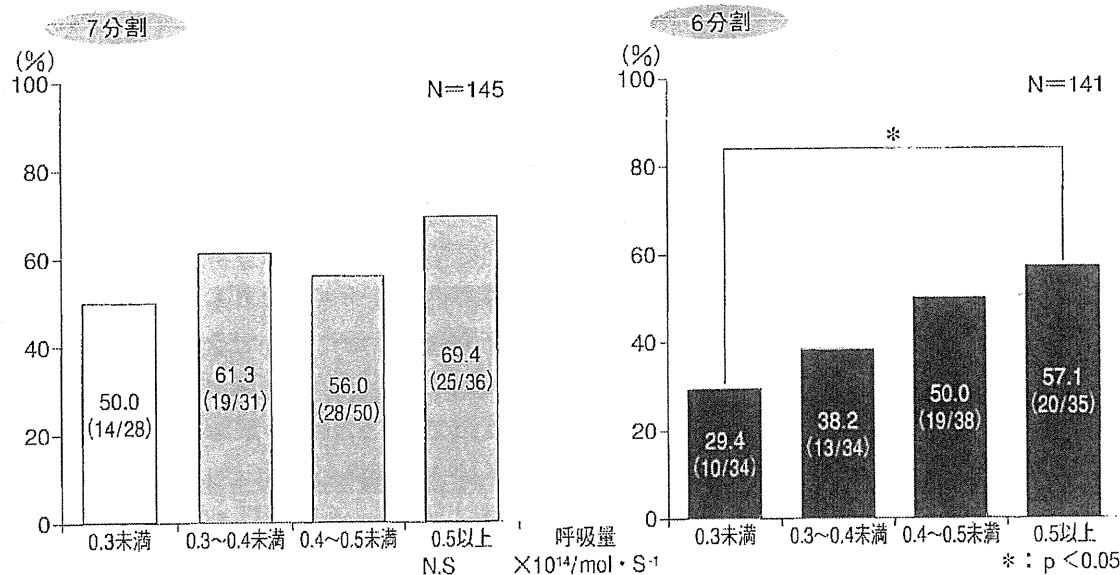


図3 分割数別にみた胚呼吸量と胚盤胞到達率

3. 検討 3

現在まで判明しているそれぞれの出生結果を示す。呼吸量評価が高く移植胚となり、妊娠が成立し、出産に至ったのは11名で、男児6名、女児5名、平均体重は2,906gだった。形態評価のみで出産に至った7名は、男児4名、女児3名、平均体重は2,720gだった。両群に有意差を認めず、呼吸量測定を行っても健全な出生を認めた。

III. 考 察

体外受精が登場して以来、妊娠率向上のため多くの施設で2個以上の胚移植が行われてきた。近年の体外受精技術の発展により、妊娠率は上昇し、それに伴い多胎率の増加も報告されている¹⁾。体外受精技術を提供しているわれわれにとって、妊娠率を低下させることなく、危険な合併症や周産期異常が危惧される多胎妊娠

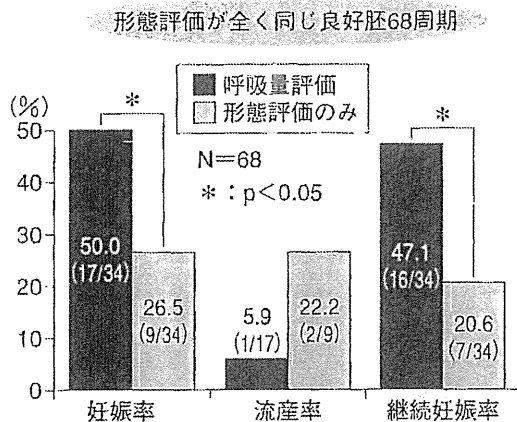


図4 選択的単一胚移植 (eSET) の妊娠率

を防ぐことは、重要な課題である。2008年2月、日本産科婦人科学会から条件付きで移植胚は原則1個とするという改定案が出された。このため最も着床能力のある1個の胚を見分けることがさらに要求される。

現在まで妊娠率向上のため多くの研究者より様々な胚の形態評価法が報告された。前核期ではZollnerら³⁾、Scottら⁴⁾、Tesarikら⁵⁾が前核の接着や核小体数の評価に基づく判定を提案している。2細胞期胚ではそれぞれの細胞の核の局在判定と早期分割による胚発生能の評価法が提案されている⁶⁾。1998年頃からは、胚の長期培養による選別法が考えられ、胚盤胞期移植が注目されるようになった。分割期と胚盤胞期移植の比較検討では、Gardnerら⁷⁾が、胚盤胞期移植で着床率は有意に上昇したと報告した。しかし、Coskunら⁸⁾やUtsumiyaら⁹⁾は、胚盤胞まで発育が進まず移植キャンセルとなった症例を含めると、妊娠率は分割期移植と有意差はないという報告もしている。これらの評価法はすべて形態評価であり、観察者の主観によって差が生じる可能性がある。このことからいまだ決定的な胚の選別方法は確立されていないと考えられる。

阿部らは、細胞活動に必要なエネルギー(ATP)を産生するミトコンドリアの酸化リン酸化反応(呼吸)に着目した¹⁰⁾¹¹⁾。胚の呼吸量を測定することにより、品質評価が可能とな

るか検討するため、非侵襲的な呼吸測定装置を開発している^{12)~14)}。これまでに、ウシ、ブタ、マウスの呼吸量解析に成功しており、胚評価への有効性を示した¹⁵⁾。そこで、われわれはヒト胚への応用を目的に、余剰胚の呼吸量測定を行った。呼吸量測定の安全性を確認するため、呼吸量測定胚および非測定胚において、胚盤胞到達率に差がないか検討したが、両群で差は認めなかった¹⁶⁾。また、胚の品質と呼吸量の関連性を検討した結果、Veeckの分類法による形態評価は呼吸量と必ずしも一致しないことを示し、呼吸量測定は、形態観察では評価できない胚の状態を数値化して示すことが可能となることを報告した¹⁷⁾。また、ミトコンドリアの発達と呼吸量の増加が一致することも明らかにされている¹⁸⁾。

以前のわれわれの検討では、移植胚の選択は呼吸量評価のみで行うより、形態評価のみで行うほうが妊娠率は高くなることを示した(形態評価のみ39.3%、呼吸量評価のみ26.7%、2008年日本生殖医学会シンポジウムにて)。そこで今回は形態評価に呼吸量評価を加えることで、形態評価のみで選ぶよりも着床能を持った1個の胚を選択することができるか検討した。当院で移植時良好胚が2個以上存在する移植胚選別困難例での、Day3時形態評価のみの胚盤胞到達率は9分割以上で67.1%、8分割は76.8%、7分割は59.3%、6分割は44.0%で8分割を示す胚で最も胚盤胞到達率が高かった。今回検討した9分割以上、7分割および6分割胚では呼吸量が大きくなるほど胚盤胞到達率は高くなる結果を示し、形態評価のみでも高率に胚盤胞へ発育する8分割では呼吸量の違いによる差は認めなかった。吉田¹⁹⁾はDay3に観察したとき、8分割を示す胚は他の分割を示す胚よりも、最も着床率が高くなることを報告しており、このことからDay3に良好な8分割を示していた胚はそれだけで十分高い発育能があることを示唆している。しかし、それ以外の胚では胚の呼吸量を測定することで、胚の品質を数値化して客観的に確認することができ、呼吸量の大きい

胚を選ぶことで、その後の発育可能な胚を見分けることが可能となる。

検討2のDay 3-eSETの検討では、前方視的検討として無作為に呼吸量を加えた群と形態評価のみで移植を行った群に振り分けたが、呼吸量を加えた群で妊娠率は高く、流産率も低くなり、それに伴い継続妊娠率が高くなる結果が得られた。形態評価がまったく等しく見える胚でもその後の発育能は異なり、このことが、呼吸量を測定することにより知りえたための結果であると考えられる。

呼吸量測定胚の出生結果でも呼吸量測定胚、非測定胚で差はみられないことが確認できた。

おわりに

胚の呼吸量を測定することは、形態評価のみでは知りえなかった胚の状態を数値化し、客観的に確認することができる。呼吸量測定を形態評価に加えることで、最も着床能のある1個の胚を選別することが可能となることが示された。

文 献

- Mullin CM, Fino ME, Talebian S, et al : Comparison of pregnancy outcomes in elective single blastocyst transfer versus double blastocyst transfer stratified by age. *Fertil Steril*, **93** : 1837-1843, 2010. Epub Feb 27, 2009.
- 那須 恵, 後藤香里, 熊迫陽子, 他 : 電気化学的呼吸計測によるヒト胚のクオリティー評価. *産婦の実際*, **57** : 289-294, 2008.
- Zollner U, Zollner KP, Hartl G, et al : The use of a detailed zygote score after IVF/ICSI to obtain good quality blastocysts : the German experience. *Hum Reprod*, **17** : 1327-1333, 2002.
- Scott L, Alvero R, Leondires M, et al : The morphology of human pronuclear embryos is positively related to blastocyst development and implantation. *Hum Reprod*, **15** : 2394-2403, 2000.
- Tesarik J, Greco E : The probability of abnormal preimplantation development can be predicted by a single static observation on pronuclear stage morphology. *Hum Reprod*, **14** : 1318-1323, 1999.
- Ciray HN, Karaqenc L, Uluq U, et al : Early cleavage morphology affects the quality and implantation potential of day 3 embryos. *Fertil Steril*, **85** : 358-365, 2006.
- Gardner DK, Schoolcraft WB, Wargley L, et al : A prospective randomized trial of blastocyst culture and transfer in *in-vitro* fertilization. *Fertil Steril*, **13** : 3434-3440, 1998.
- Coskun S, Hollanders J, Al-Hassan S, et al : Day 5 versus day 3 embryo transfer : a controlled randomized trial. *Hum Reprod*, **15** : 1947-1952, 2000.
- Utsunomiya T, Ito H, Nagaki M, et al : A Prospective, Randomized Study : Day-3 versus Hatching Blastocyst Stage. *Hum Reprod*, **19** : 1598-1603, 2004.
- Abe H, Matsuzaki S, Hoshi H : Ultrastructural differences in bovine morulae classified as high and low qualities by morphological evaluation. *Theriogenology*, **57** : 1273-1283, 2002.
- 阿部宏之 : 電気化学的イメージング技術を応用した胚のクオリティー評価. *産婦の実際*, **55** : 207-216, 2006.
- Abe H, Shiku H, Aoyagi S, et al : *In vitro* culture and evaluation of embryos for production of high quality bovine embryos. *J Mamm Ova Res*, **21** : 22-30, 2004.
- Shiku H, Shiraishi T, Ohya H, et al : Oxygen consumption of single bovine embryos probed with scanning electrochemical microscopy. *Anal Chem*, **73** : 3751-3758, 2001.
- Shiku H, Shiraishi T, Aoyagi S, et al : Respiration activity of single bovine embryos entrapped in a cone-shaped microwell monitored by scanning electrochemical microscopy. *Anal Chim Acta*, **522** : 51-58, 2004.
- Abe H, Shiku H, Yokoo M, et al : Evaluating the quality of individual embryos with a non-invasive and highly sensitive measurement of oxygen consumption by scanning electrochemical microscopy. *J Reprod Dev*, **52** (Suppl) : S55-S64, 2006.
- 後藤香里, 小池 恵, 熊迫陽子, 他 : 電気化学的呼吸計測技術におけるヒト胚クオリティー評価と安全性. *日受精着床会誌*, **27** : 53-58, 2010.
- Utsunomiya T, Goto K, Nasu M, et al : Evaluating the quality of human embryos with a measurement of oxygen consumption by scanning electrochemical microscopy. *J Mamm Ova Res*, **25** : 2-7, 2008.
- 阿部宏之, 横尾正樹, 荒木康久, 他 : 電気化学的イメージング法を応用した単一ヒト胚の呼吸能解析. *産婦の実際*, **56** : 2053-2057, 2007.
- 吉田 淳 : 胚の選別と胚移植, *ART 実践マニュアル*, p 63, 永井書店, 2005.

Influence of Tip Size on Single Yeast Cell Imaging Using Scanning Electrochemical Microscopy

Kuniaki Nagamine, Yasufumi Takahashi, Kosuke Ino, Hitoshi Shiku, Tomokazu Matsue*

Graduate School of Environmental Studies, Tohoku University, 6-6-11, Aramaki-Aoba, Aoba, Sendai 980-8579, Japan

tel/fax: +81-22-795-7209

*e-mail: matsue@bioinfo.che.tohoku.ac.jp

Received: September 24, 2010

Accepted: January 10, 2011

Abstract

The influence of the tip reaction on the substrate generation/tip collection mode SECM imaging of a single yeast cell was investigated by using various sizes of probe electrodes in μm – nm scales because the tip reaction would disturb the concentration profile of intracellular enzyme reactant formed around the cell. GC mode measurements of a single yeast cell were performed using a dual mediator system with lipophilic menadione and hydrophilic ferricyanide. We found downscaling of the tip size enabled quantitative SECM imaging of a single cell in GC mode without disturbing the concentration profile of the mediator formed around the cell by the tip reaction.

Keywords: Scanning electrochemical microscopy, Nanoelectrodes, Single cell analysis

DOI: 10.1002/elan.201000595

1 Introduction

Quantitative analysis of intracellular enzyme activity in microbial cells including yeast cells has been required for investigation of cell physiology and cell-based diagnosis of pathologic conditions. In particular, measurement of cellular activity of a specific cell spatially localized in a densely packed cell population is helpful for revealing metabolic alteration in individual cells via cell-cell communication. This metabolic regulation is a requisite for microbial cells to survive in variable and cruel microenvironments and for some bacteria to induce pathogenic gene expression [1–4]. Therefore, development of single microbial cell analysis in a densely packed population has been expected to reveal the cell-cell communication in microbial cells and to improve the screening drugs used to inhibit pathogenic gene expression in an infectious cell.

Bioelectrochemical methods have provided the noninvasive quantitative analysis of intracellular redox enzyme activity using mediators that shuttle electrons between intracellular enzymes and the electrode placed extracellularly [5–10]. In addition, by means of scanning electrochemical microscopy (SECM), intracellular enzyme activity has been quantified in spatially localized single prokaryotic and eukaryotic cells [11–27]. In substrate generation/tip collection (GC) mode SECM, a concentration profile of intracellular enzyme reactant was detected by scanning a probe electrode above a target cell. Sensitivity of GC mode SECM is relatively high as the background signal is very low. However, when a probe electrode with a large active tip was used for GC mode imaging, the concentration profile of intracellular enzyme reactant formed

around the cells might be disturbed by the consumption (or generation) of redox species at the tip itself. Downscaling of the tip size would suppress the disturbance of concentration profile and enables clear imaging of a single cell.

In this study, we investigated the influence of tip reaction on the GC mode SECM imaging of a single yeast cell by using various Pt electrode probes with tip sizes in μm – nm scales. The target intracellular enzyme was cytosolic and mitochondrial NAD(P)H-oxidizing enzymes (NOEs), which is the general term for all enzymes catalyzing electron transfer from NAD(P)H to quinone substrates. Figure 1 shows the principle of electrochemical detection of NOEs activity in the GC mode [5–10]. NOEs activity in a yeast cell was detected using a dual mediator system with lipophilic menadione and hydrophilic ferricyanide. Mauzeroll and Bard investigated the permeation of menadione through yeast cells, the intracellular formation of menadione-*S*-glutathione conjugate, and the efflux of the conjugate from the cells using GC mode SECM [28]. In this study, menadione shuttles electrons from intracellular NOEs to extracellular ferricyanide with low permeability to cell membrane, followed by ferrocyanide generation around the cell. SECM was used to monitor the ferrocyanide generation that reflects NOEs activity in yeast cell. We found that downscaling of the tip size enabled quantitative SECM imaging of a single yeast cell in GC mode without disturbing the concentration profile of mediator formed around the cell by the tip reaction.

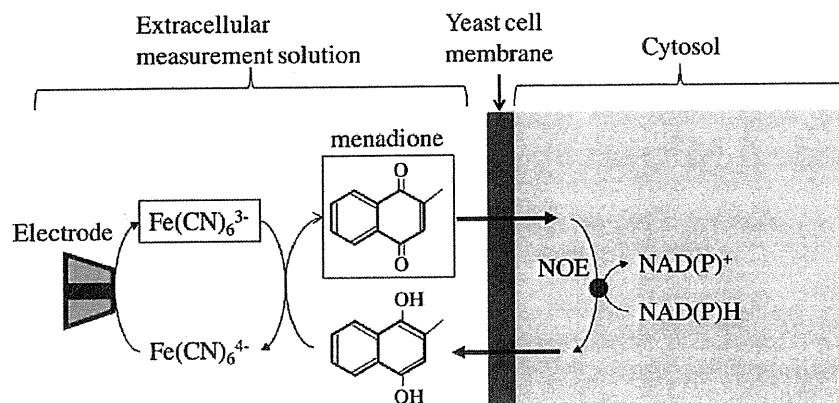


Fig. 1. Principle of electrochemical detection of NOEs activity in yeast cell. $\text{Fe}(\text{CN})_6^{3-}$ and menadione (indicated by squares) were added to the measurement solution.

2 Experimental

2.1 Reagents

Potassium hexacyanoferrate(III), menadione, D-(+)-glucose were purchased from Wako Pure Chemicals Industries, Ltd. Ferrocene methanol (FcCH_2OH) was purchased from Sigma Aldrich. All solutions were prepared using distilled and deionized water from Direct-Q (Millipore).

2.2 Yeast Strain and Growth Conditions

Saccharomyces cerevisiae strain Y190 was donated by Dr. Fujio Shiraishi from the National Institute for Environmental Studies. The cells were cultured for 24 h at 30 °C with shaking at 100 rpm in modified SD medium (without tryptophan and leucine) [17]. The culture was collected as a pellet by centrifugation (6000 rpm for 5 min), washed twice with Z buffer (60.0 mM $\text{Na}_2\text{HPO}_4 \cdot 12\text{H}_2\text{O}$; 39.7 mM $\text{NaH}_2\text{PO}_4 \cdot 2\text{H}_2\text{O}$; 10.0 mM KCl; 10.0 mM $\text{MgSO}_4 \cdot 7\text{H}_2\text{O}$; pH 7.0), and then resuspended in Z buffer.

2.3 Fabrication of Pt Micro- and Nanoelectrodes

The fabrication of the Pt microelectrode was described previously [29]. A Pt nanoelectrode was fabricated by simultaneously pulling a quartz capillary and a Pt wire inserted into the capillary under vacuum using a CO_2 laser puller P-2000 (Sutter) [30–32]. First, an annealed Pt wire (25.0 μm diameter) was inserted into the middle of 100 mm long quartz capillary (1.0 mm outer diameter and 0.3 mm inner diameter). Then, the Pt wire was sealed into the quartz capillary by irradiating CO_2 laser to the middle of the capillary under the following parameters: heat = 960, filament = 4, velocity = 100, delay = 120 and pull = 0. The heating process was carried out for 30 s followed by a cooling time of 30 s. For tight sealing of the Pt wire into the capillary, the heating process was performed under reduced pressure by connecting each end of the

quartz capillary to a vacuum line. The heating/cooling process was repeated 5 times to ensure a proper sealing. Later, the capillary was pulled under the following parameters to form two sets of Pt nanoelectrodes: heat = 885, filament = 2, velocity = 50, delay = 100, and pull = 100. A copper lead wire was inserted into the capillary to make an electrical connection with the Pt wire using a silver paste. Finally, the tip of the nanoelectrode was carefully polished using a diamond grinder (EG-6, Narishige) to expose the disk-shaped active surface of the Pt wire.

2.4 SECM Imaging of NOEs Activity in Bulk Yeast Cells

Yeast cells (4×10^4) were entrapped in a cylindrical-shaped poly(dimethylsiloxane) (PDMS) microwell (diameter, 450 μm ; depth, 50 μm). The fabrication method of the PDMS microwell array has been described previously [17]. The suspension of yeast cells was dispersed on the PDMS microwell array and stabilized for 10 min until the cells were dropped into the wells. The excess yeast cells were removed by washing the surface of the PDMS microwell array with Z buffer two times. Finally, the measurement solution was poured on the PDMS microwell array for SECM measurements. The components of the measurement solution were as follows: 20 mM potassium hexacyanoferrate(III), 0.10 mM menadione, and 20 mM D-(+)-glucose in Z buffer.

Imaging experiments were carried out using a SECM system including an inverted microscope (TE300, Nikon), a current amplifier (Model 427, Keithley), a stepping motor-driven XY stage (Model D70, Suruga Seiki), and a piezoelectric motor-driven Z stage (E-501, Physik Instrumente). For positioning, the Pt probe microelectrode (Pt radius, 7.4 μm) was brought into contact with the substrate surface. From there the probe was vertically retracted 20.0 μm off the surface using the piezoelectric motor with a precision of 0.1 μm . The potential of the probe electrode was held at +0.60 V vs. Ag/AgCl to provide a steady-state oxidation current for reduced form of mediator. The electrode was vertically scanned from the

original set position to 1.0 mm away from the PDMS surface at a scan rate of $9.5 \mu\text{m s}^{-1}$ to detect the ferrocyanide concentration profile formed around the microwell containing yeast cells.

2.5 SECM Imaging of NOEs Activity in Single or Several Yeast Cells

Single or groups of yeast cells were electrostatically immobilized on an aminosilanized glass (Matsunami Glass Ind. Ltd.). The suspension of yeast cells was dispersed on the glass substrate and stabilized for 10 min to allow attachment on the surface of the glass. Excess yeast cells were removed by washing the surface of the slide glass with Z buffer twice, followed by pouring the measurement solution on the slide glass. The measurement solution was Z buffer containing 20 mM potassium hexacyanoferrate(III), 0.10 mM menadione, and 20 mM D-(+)-glucose. The Pt probe micro- or nanoelectrode was positioned 7.0 μm above the substrate surface with a precision of 0.1 μm in vertical direction. The probe electrode was laterally scanned over yeast cells at a scan rate of $1.0 \mu\text{m s}^{-1}$ to detect the concentration profile of ferrocyanide around the cells. The potential of the probe electrode was held at +0.60 V vs. Ag/AgCl to detect the oxidation current for ferrocyanide. The time required for SECM imaging at an area of $30 \times 30 \mu\text{m}^2$ (spatial resolution, 1.0 μm) was approximately 30 min.

2.6 Quantitative Analysis of Mass Transfer Rate of Redox Mediator from Single Yeast Cell Using GC Mode SECM Imaging

Quantification of the mass transfer rate of the redox mediator from single yeast cell was carried out using GC mode SECM imaging as described previously [33]. When a spherically shaped cell is positioned on a flat substrate in a measurement solution, the mass transfer rate of the hemispherically diffusing redox mediator from the yeast cell (F_{yeast} in mols^{-1}) in a steady-state rate can be estimated by multiplying the flux at a certain point ($f_{r=rx}$ in $\text{mol cm}^{-2} \text{s}^{-1}$, r refers to the distance from the cell surface) with the semi-spherical section area ($S_{r=rx}$ in cm^2)

$$F_{\text{yeast}} = f_{r=rx} \times S_{r=rx} \quad (1)$$

The $S_{r=rx}$ value is expressed as follows:

$$S_{r=rx} = 2\pi r_x^2 \quad (2)$$

At $r=r_x$, the flux is expressed as

$$f_{r=rx} = D (\Delta C_{r=rx} / \Delta r) \quad (3)$$

Where D is the diffusion coefficient of a redox mediator (for ferrocyanide, $D_{\text{ferro}} = 6.5 \times 10^{-6} \text{ cm}^2 \text{ s}^{-1}$); $\Delta C_{r=rx} / \Delta r$ is the concentration gradient of the redox mediator, and $\Delta C_{r=rx}$ and Δr are expressed as

$$\Delta C_{r=rx} = |C_{r=rx} - C_{r=rx+\Delta r}| \quad (4)$$

$$\Delta r = |r_{r=rx} - r_{r=rx+\Delta r}| \quad (5)$$

The concentration gradient of a redox mediator at $r=r_x$ is calculated from the profiles of the redox current. The redox current observed with the SECM system is expressed by

$$I_{r=rx} = 4nFD C_{r=rx} a \quad (6)$$

Where n is the number of electrons per molecule reduced; F is the Faraday constant (96500 C mol^{-1}); $C_{r=rx}$ is the local concentration of the redox mediator at $r=r_x$ (mol cm^{-3}); and a is the electrode radius (cm).

For SECM imaging using a dual mediator system, it was assumed that menadione is localized within the yeast cell and ferricyanide is outside of the cell. When the ferricyanide concentration is in large excess over the menadione concentration, menadione should not be detected directly with a SECM probe electrode because all the menadione is reoxidized by ferricyanide at the cell surface. If we assume that the concentration of menadione and ferricyanide is in large excess over the Michaelis constant value of NOEs and that the SECM probe detects the diffusion-limited current, the rate-limiting step for determining current response is the cellular reaction step including NOEs reaction rate and the permeation rate of mediator through the cell membrane [34].

3 Results and Discussion

Figure 2A shows the scanning electron micrograph (SEM) of the tip of the Pt nanoelectrode. The nanometer-sized Pt disk was clearly identified at the center of the insulating quartz sheath. At higher magnification, the radius of the Pt disk was determined to be approximately 300 nm (Figure 2B). Figure 2C shows a cyclic voltammogram (CV) of 0.50 mM FcCH_2OH detected with the Pt nanoelectrode shown in Figure 2A. At the potential scan rate of 20 mV/s, CV showed a s-shaped curve with the steady-state current at +0.50 V vs. Ag/AgCl. Assuming the geometry of the nanoelectrode to be disk shaped, the steady-state current for a nanoelectrode in an insulating sheath is given by Equation 6 with the diffusion coefficient of FcCH_2OH as $7.8 \times 10^{-6} \text{ cm}^2 \text{ s}^{-1}$ [32] and the bulk concentration of FcCH_2OH as $5.0 \times 10^{-7} \text{ mol cm}^{-3}$. Using Equation 6, the radius of the nanoelectrode was calculated as 380 nm, which was almost the same size as the identified size from SEM observation.

Figure 3A shows the responses of 4×10^4 yeast cells entrapped in a PDMS microwell in 20 mM D-(+)-glucose solution containing (a) 20 mM ferricyanide, (b) 0.10 mM menadione, and (c) 20 mM ferricyanide and 0.10 mM menadione. The ordinate in Figure 3A represents the current change when the electrode set at +0.60 V vs. Ag/AgCl was vertically scanned from the original set position

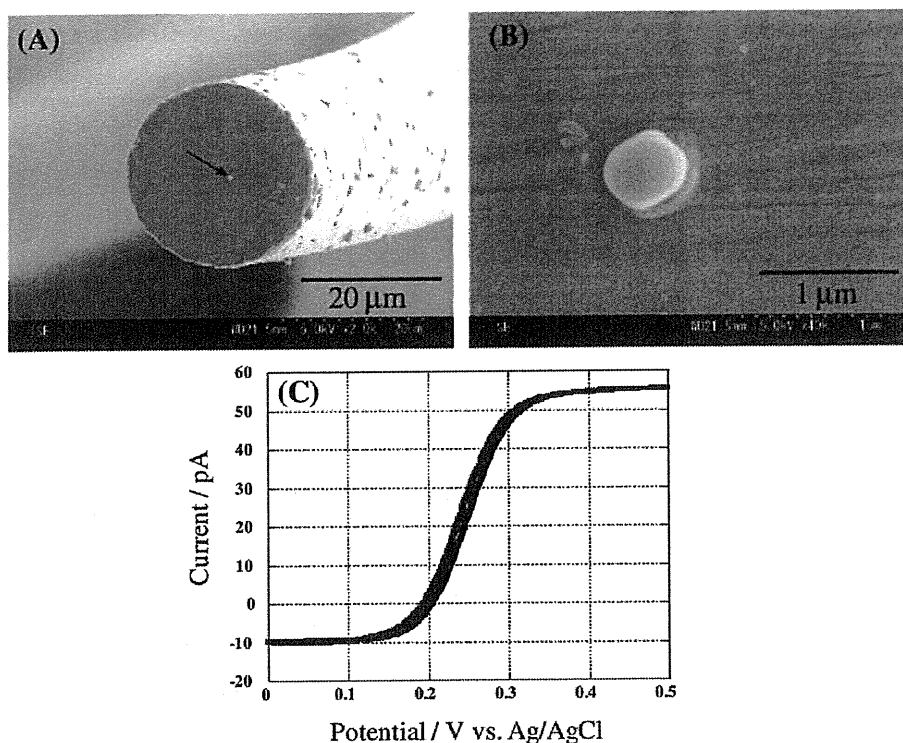


Fig. 2. A) Scanning electron micrograph of the tip of a Pt nanoelectrode. B) Pt disk of the same nanoelectrode as (A) at a higher magnification. C) Cyclic voltammogram of 0.50 mM FcCH_2OH using the Pt nanoelectrode shown in (A). Scan rate: 20 mV s^{-1} .

(20.0 μm above the PDMS well surface) to 1.0 mm above from the well surface. When the solution contained only ferricyanide (Figure 3Aa), the current change was only several pA and almost no current variation was observed on scanning the electrode. This suggests almost no interaction of ferricyanide with the intracellular redox processes due to low permeability of hydrophilic ferricyanide through the yeast cell membrane. In the case of lipophilic menadione (Figure 3Ab), on the other hand, the current change became larger (48 pA). Menadione functions as a permeable redox mediator to interact with NOEs to form menadiol which diffuses into the solution to reduce ferricyanide to give oxidation current at the electrode probe (see Figure 1) [9]. In a dual mediator system (Figure 3Ac), the current change was 2.3 times higher than that with menadione alone in the solution. This tendency was in accordance with previous reports [5,6,9], which suggested that the enhancement of current change in the dual mediator system would attribute to the redox cycling reaction of menadione between ferricyanide and intracellular NOEs depicted in Figure 1 and the help of ferricyanide to overcome the slow heterogeneous redox kinetics of menadione on Pt electrodes [9].

For quantitative analysis of the mass transfer rate of the ferrocyanide from single yeast cell, we examined the concentration of the mediators in large excess over the Michaelis constant value of NOEs. Figure 3B shows the relationship between the mediator concentration and the current change in a dual mediator system. The current

change was detected as described in Figure 3A. Each point in Figure 3B has relatively large error bar, because the differences in individual cellular activity caused variation of averaged activity of the cell population depending on the microenvironmental conditions. In Figure 3Ba, the current change tended to be saturated when the concentration of ferricyanide was higher than 1.0 mM in the presence of 0.10 mM menadione. When it was assumed that all of the 1.0 mM ferricyanide was reduced to ferrocyanide by menadiol and the ferrocyanide was oxidized at the 7.4 μm-radius tip in the bulk solution, the calculated oxidation current for ferrocyanide using the Equation 6 is 1.86 nA. This value is much larger than the current change for ferrocyanide generated from the cells in Figure 3Ac (48 pA) even when using 20 mM ferricyanide. These results suggested that more than 1.0 mM of ferricyanide concentration is in large excess over the Michaelis constant value of NOEs. In Figure 3Bb, the current changes increased with increase the menadione concentration and retarded at the concentration higher than 0.20 mM in the presence of 20 mM ferricyanide. Then, the current change gradually decreased when the cells were exposed to the solution containing more than 0.20 mM menadione. This behavior suggests the cytotoxicity of menadione or rapid exhaustion of NAD(P)H [9]. On the basis of these results, the concentrations of menadione and ferricyanide were set to 0.10 mM and 20 mM, respectively, for the dual mediator system.

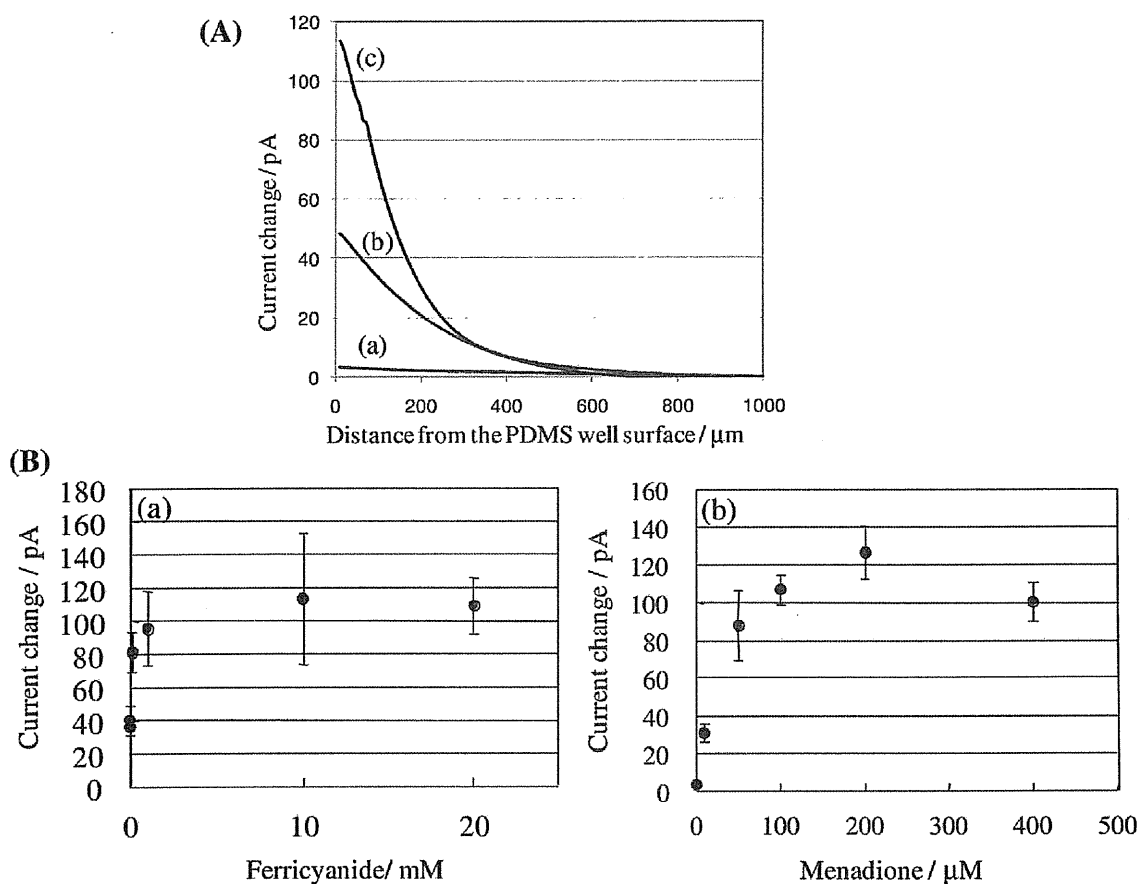


Fig. 3. A) Current changes when a Pt microelectrode probe retracted from 20 μm to 1.0 mm above from the PDMS microwell surface entrapped with 4×10^4 yeast cells in 20 mM D-(+)-glucose solution containing (a) 20 mM ferricyanide, (b) 0.10 mM menadione, and (c) 20 mM ferricyanide and 0.10 mM menadione. B) Current changes vs. concentration plots for (a) ferricyanide and (b) menadione. (a): Concentration of menadione was set at 0.10 mM. (b): Concentration of ferricyanide was set at 20 mM. Each point represents the mean of five measurements \pm SD. Probe: Pt microelectrode with Pt radius of 7.4 μm . Potential of the probe: +0.60 V vs. Ag/AgCl.

Figure 4 shows the line scan responses for the dual mediator system of 4 aggregated yeast cells when a probe electrode with a Pt radius of (a) 11.9 μm , (b) 1.0 μm , or (c) 199 nm was scanned 7.0 μm above the surface of the glass substrate, together with the optical image of the cells. All the lines show peaks of oxidation current corresponding to the NOEs activity of yeast cells, although the change in the current from the baseline became small with decreasing tip size. The generation rate of ferrocyanide from a single yeast cell, F_{yeast} , was calculated based on Equation 1 and was found to be 3.07×10^{-19} (11.9- μm tip), 1.69×10^{-19} (1.0- μm tip), and 1.73×10^{-19} (199-nm tip) $\text{mols}^{-1} \text{cell}^{-1}$. The generation rates detected using probes with 1.0 μm or 199 nm radii were almost identical and in good agreement with the value previously reported [5]. The oxidation rate for ferrocyanide at the probe electrode, F_{tip} , was calculated based on Equation 6 and found to be 8.05×10^{-20} (1.0- μm tip) and 1.73×10^{-20} (199-nm tip) mols^{-1} at the peaks in Figure 4B. As F_{tip} at the 199-nm tip was sufficiently smaller than F_{yeast} , the ferrocyanide concentration profile around the cells would not be dis-

turbed by the electrochemical reaction at the tip. However, each single cellular activity could not be resolved from the current response due to crossover of the ferrocyanide diffusion layers around the yeast cells. For the 11.9- μm tip, a large amount of ferrocyanide generated from a yeast cell would be consumed at the probe electrode ($F_{\text{tip}} = 1.63 \times 10^{-18} \text{ mols}^{-1}$). Therefore, local concentrations of ferrocyanide could not be precisely measured.

The signal-to-noise ratios in Figure 4B were 23.0 (signal = 668.1 fA, noise = 29.0 fA) for the 11.9- μm tip, 1.7 (signal = 29.0 fA, noise = 17.2 fA) for the 1.0- μm tip, 0.5 (signal = 14.3 fA, noise = 27.1 fA) for the 199-nm tip. Although the noise is in the range of the signal when using nanoelectrode, the increase of oxidation current for ferrocyanide was reproducibly detected around the yeast cells, suggesting the significant current response of the cells was detected using nanoelectrode.

The SECM measurements enabled the visualization of NOEs activity of an isolated single cell. Figure 5 shows the SECM image of a single yeast cell based on oxidation current for ferrocyanide in dual mediator system with the

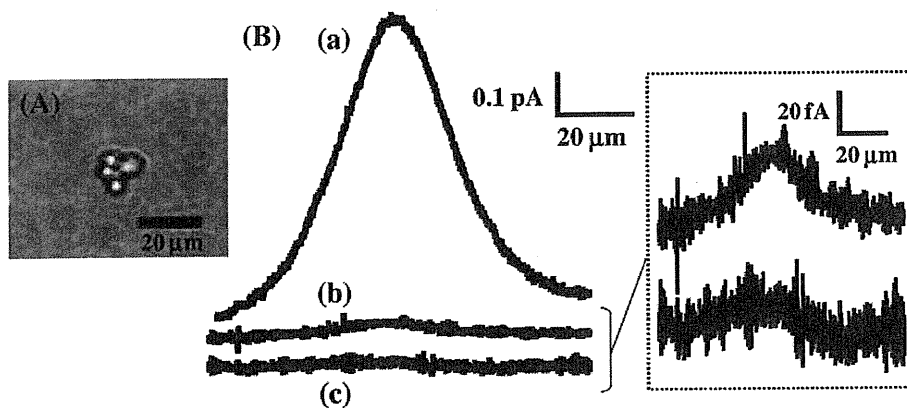


Fig. 4. A) The micrograph of 4 yeast cells. B) Current responses in line-scan images for 4 yeast cells in 20 mM D-(+)-glucose solution containing 20 mM ferricyanide and 0.10 mM menadione. Probe: Pt electrode with a Pt radius of (a) 11.9 μm , (b) 1.0 μm , and (c) 199 nm. Scan rate: 1.0 $\mu\text{m s}^{-1}$. Potential of the probe: +0.60 V vs. Ag/AgCl.

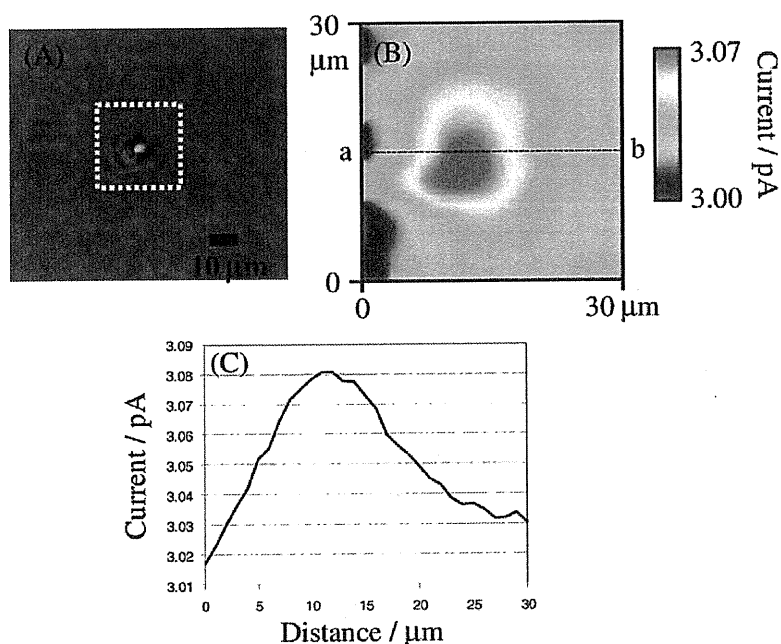


Fig. 5. A) Micrograph of a single yeast cell. B) SECM image of single yeast cell based on oxidation current for ferrocyanide in 20 mM D-(+)-glucose solution containing 20 mM ferricyanide and 0.10 mM menadione. C) Line scan along the cross section a-b in Figure 5B. Probe: Pt nanoelectrode with the Pt radius of 450 nm. Potential of the probe: +0.60 V vs. Ag/AgCl. Scan rate: 1.0 $\mu\text{m s}^{-1}$.

electrode probe of 450 nm-tip, together with an optical image of the cell. The enhanced current around the cell clearly indicated the NOEs activity of the yeast cell in Figure 5B. Figure 5C shows the line scan along the cross section a-b in Figure 5B. The signal-to-noise ratio calculated from the line scan was 7.7 (signal = 63.7 fA, noise = 8.24 fA), suggesting a significant response of the single yeast cell. Half-width of the current profile for ferrocyanide was found to be 14 μm , which was significantly larger than the size of yeast cell (5.0 μm in diameter). It should be noted again that, regardless of tip diameter, single-cell level resolution in cell aggregates is difficult in the present constant-height GC mode SECM imaging due

to spread of the ferrocyanide diffusion layer around the cell.

4 Conclusions

Influence of tip reaction on the GC mode SECM imaging of a single yeast cell was investigated by using various Pt electrode probes with tip sizes in μm -nm scales. The quantitative imaging of NOEs activity in an isolated yeast cells was successfully achieved in the GC mode measurements using the 199 nm-tip without disturbing the mediator concentration profile formed around the cells by the

tip reaction. However, spatial resolution of the SECM image was not improved even when the tip size was downscaled due to spread of the ferrocyanide diffusion layer around the cell. To obtain higher resolution of single cellular images in GC mode, one has to incorporate an accurate cell-benign distance control mechanism at nanometer scale into the SECM system. We think a shear-force or an ion-conductance feedback control is the probable candidate for the distance control. Using these distance control mechanisms, topographic and electrochemical images of locally immobilized cells were captured simultaneously in nanometer-order resolution using standing approach mode SECM [19–22]. In the future, the SECM system with a cell-benign distance control will be applied for characterization of single live yeast cells in a densely-packed population.

Acknowledgements

This work was partly supported by Grants-in-Aid for Scientific Research (18101006, 9750055, 22245011) from MEXT (Ministry of Education, Culture, Sports, Science and Technology), Japan and by a grant from the Center for Interdisciplinary Research, Tohoku University. K. N. acknowledges G-COE.

References

- [1] M. A. Aon, S. Cortassa, K. M. Lemar, A. J. Hayes, D. Lloyd, *FEBS Lett.* **2007**, *581*, 8.
- [2] D. B. Murray, M. Beckmann, H. Kitano, *Proc. Natl. Acad. Sci. USA* **2007**, *104*, 2241.
- [3] Z. Palkova, L. Vachova, *FEMS Microbiol. Rev.* **2006**, *30*, 806.
- [4] C. T. Parker, V. Sperandio, *Cell. Microbiol.* **2009**, *11*, 363.
- [5] K. H. R. Baronian, A. J. Downard, R. K. Lowen, *Appl. Microbiol. Biotechnol.* **2002**, *60*, 108.
- [6] A. Heiskanen, J. Yakovleva, C. Spegel, R. Taboryski, M. Koudelka-Hep, J. Emneus, T. Ruzgas, *Electrochem. Commun.* **2004**, *6*, 219.
- [7] A. Heiskanen, C. Spegel, N. Kostesha, S. Lindahl, T. Ruzgas, J. Emneus, *Anal. Biochem.* **2009**, *384*, 11.
- [8] J. D. Rabinowitz, J. F. Vacchino, C. Beeson, H. M. McConnell, *J. Am. Chem. Soc.* **1998**, *120*, 2464.
- [9] C. F. Spegel, A. R. Heiskanen, N. Kostesha, T. H. Johanson, M. F. G. Grauslund, M. Koudelka-Hep, J. Emnus, T. Ruzgas, *Anal. Chem.* **2007**, *79*, 8919.
- [10] J. Zhao, M. Wang, Z. Yang, Z. Wang, H. Wang, Z. Yang, *Anal. Chim. Acta* **2007**, *597*, 67.
- [11] C. Amatore, S. Arbault, M. Erard, *Anal. Chem.* **2008**, *80*, 9635.
- [12] C. Cai, B. Liu, M. V. Mirkin, H. A. Frank, J. F. Rusling, *Anal. Chem.* **2002**, *74*, 114.
- [13] W. Feng, S. A. Rotenberg, M. V. Mirkin, *Anal. Chem.* **2003**, *75*, 4148.
- [14] D. T. Pierce, A. J. Bard, *Anal. Chem.* **1993**, *65*, 3598.
- [15] H. Shiku, T. Shiraishi, H. Ohya, T. Matsue, H. Abe, H. Hoshi, M. Kobayashi, *Anal. Chem.* **2001**, *73*, 3751.
- [16] H. Shiku, T. Shiraishi, S. Aoyagi, Y. Utsumi, M. Matsudaira, H. Abe, H. Hoshi, S. Kasai, H. Ohya, T. Matsue, *Anal. Chim. Acta* **2004**, *522*, 51.
- [17] H. Shiku, S. Goto, S. Jung, K. Nagamine, M. Koide, T. Itayama, T. Yasukawa, T. Matsue, *Analyst* **2009**, *134*, 182.
- [18] P. Sun, F. O. Laforge, T. P. Abeyweera, S. A. Rotenberg, J. Carpino, M. V. Mirkin, *Proc. Natl. Acad. Sci. USA* **2008**, *105*, 443.
- [19] Y. Takahashi, Y. Hirano, T. Yasukawa, H. Shiku, H. Yamada, T. Matsue, *Langmuir* **2006**, *22*, 10299.
- [20] Y. Takahashi, T. Miyamoto, H. Shiku, R. Asano, T. Yasukawa, I. Kumagai, T. Matsue, *Anal. Chem.* **2009**, *81*, 2785.
- [21] Y. Takahashi, H. Shiku, T. Murata, T. Yasukawa, T. Matsue, *Anal. Chem.* **2009**, *81*, 9674.
- [22] Y. Takahashi, A. I. Shevchuk, P. Novak, Y. Murakami, H. Shiku, Y. E. Korchev, T. Matsue, *J. Am. Chem. Soc.* **2010**, *132*, 10118.
- [23] T. Yasukawa, Y. Kondo, I. Uchida, T. Matsue, *Chem. Lett.* **1998**, *8*, 767.
- [24] T. Yasukawa, I. Uchida, T. Matsue, *Biochim. Biophys. Acta, Biomemb.* **1998**, *1369*, 152.
- [25] T. Yasukawa, I. Uchida, T. Matsue, *Biophys. J.* **1999**, *76*, 1129.
- [26] L. Zhu, N. Gao, X. Zhan, W. Jin, *Talanta* **2008**, *77*, 804.
- [27] R. Zhu, S. M. Macfie, Z. Ding, *Anal. Chem.* **2008**, *24*, 14261.
- [28] J. Mauzeroll, A. J. Bard, *Proc. Natl. Acad. Sci. USA* **2004**, *101*, 7862.
- [29] T. Matsue, S. Koike, T. Abe, T. Itabashi, I. Uchida, *Biochim. Biophys. Acta* **1992**, *1101*, 69.
- [30] B. B. Katemann, W. Schuhmann, *Electroanalysis* **2002**, *14*, 22.
- [31] Y. Shao, M. V. Mirlin, G. Fish, S. Kokotov, D. Palanker, A. Lewis, *Anal. Chem.* **1997**, *69*, 1627.
- [32] P. Sun, M. V. Mirkin, *Anal. Chem.* **2006**, *78*, 6526.
- [33] T. Kaya, D. Numai, K. Nagamine, S. Aoyagi, H. Shiku, T. Matsue, *Analyst* **2004**, *129*, 529.
- [34] K. Nagamine, T. Kaya, T. Yasukawa, H. Shiku, T. Matsue, *Sens. Actuators B* **2005**, *108*, 676.

Simultaneous Noncontact Topography and Electrochemical Imaging by SECM/SICM Featuring Ion Current Feedback Regulation

Yasufumi Takahashi,[†] Andrew I. Shevchuk,[‡] Pavel Novak,[‡] Yumi Murakami,[†]
Hitoshi Shiku,[†] Yuri E. Korchev,^{*,‡} and Tomokazu Matsue^{*,†}

Graduate School of Environmental Studies, Tohoku University, Aramaki Aoba 6-6-11-605,
Sendai 980-8579, Japan, and Division of Medicine, Imperial College London, Hammersmith
Hospital Campus, London W12 0NN, United Kingdom

Received April 9, 2010; E-mail: matsue@bioinfo.che.tohoku.ac.jp

Abstract: We described a hybrid system of scanning electrochemical microscopy (SECM) and scanning ion conductance microscopy (SICM) with ion current feedback nanopositioning control for simultaneous imaging of noncontact topography and spatial distribution of electrochemical species. A nanopipette/nanoring electrode probe provided submicrometer resolution of the electrochemical measurement on surfaces with complex topology. The SECM/SICM probe had an aperture radius of 220 nm. The inner and outer radii of the SECM Au nanoring electrode were 330 and 550 nm, respectively. Characterization of the probe was performed with scanning electron microscopy (SEM), cyclic voltammetry (CV), and approach curve measurements. SECM/SICM was applied to simultaneous imaging of topography and electrochemical responses of enzymes (horse radish peroxidase (HRP) and glucose oxidase (GOD)) and single live cells (A6 cells, superior cervical ganglion (SCG) cells, and cardiac myocytes). The measurements revealed the distribution of activity of the enzyme spots on uneven surfaces with submicrometer resolution. SECM/SICM acquired high resolution topographic images of cells together with the map of electrochemical signals. This combined technique was also applied to the evaluation of the permeation property of electroactive species through cellular membranes.

Introduction

A high temporal and spatial resolution analytical tool working in physiological conditions is needed to evaluate the relationship of the localized topography and function of biomolecules. Scanning electrochemical microscopy (SECM) uses a micro- or nanoelectrode as a scanning probe and provides sample surface electrochemical property under physiological conditions without physical contact. SECM has been applied for evaluating the enzyme^{1–6} and cellular activity,^{7,8} estimating cell membrane permeability,^{9–18} and detecting electroactive metabolic chemi-

cals with short life spans, such as neurotransmitters^{19,20} and nitric oxide (NO)²¹ in the vicinity of living cellular surfaces. Membrane protein has also been detected with SECM.²² Miniaturization of the probe electrode is important for improving the temporal and spatial resolution. In addition, a fine distance regulation system is required to approach the probe electrode against live cell surfaces.

[†] Tohoku University.

[‡] Imperial College London.

- Wittstock, G. *Fresenius J. Anal. Chem.* **2001**, *370*, 303–315.
- Luo, H. Q.; Shiku, H.; Kumagai, A.; Takahashi, Y.; Yasukawa, T.; Matsue, T. *Electrochem. Commun.* **2007**, *9*, 2703–2708.
- Lei, R.; Stratmann, L.; Schafer, D.; Erichsen, T.; Neugebauer, S.; Li, N.; Schuhmann, W. *Anal. Chem.* **2009**, *81*, 5070–5074.
- Schafer, D.; Maciejewska, M.; Schuhmann, W. *Biosens. Bioelectron.* **2007**, *22*, 1887–1895.
- Maciejewska, M.; Schafer, D.; Schuhmann, W. *Electroanalysis* **2006**, *18*, 1916–1928.
- Hussien, E. M.; Erichsen, T.; Schuhmann, W.; Maciejewska, M. *Anal. Bioanal. Chem.* **2008**, *391*, 1773–1782.
- Li, X.; Bard, A. J. *J. Electroanal. Chem.* **2009**, *628*, 35–42.
- Takahashi, Y.; Hirano, Y.; Yasukawa, T.; Shiku, H.; Yamada, H.; Matsue, T. *Langmuir* **2006**, *22*, 10299–10306.
- Yasukawa, T.; Uchida, I.; Matsue, T. *Biochim. Biophys. Acta Biomembr.* **1998**, *1369*, 152–158.
- Barker, A. L.; Macpherson, J. V.; Slevin, C. J.; Unwin, P. R. *J. Phys. Chem. B* **1998**, *102*, 1586–1598.

- Gonsalves, M.; Barker, A. L.; Macpherson, J. V.; Unwin, P. R.; O'Hare, D.; Winlove, C. P. *Biophys. J.* **2000**, *78*, 1578–1588.
- Cannan, S.; Zhang, J.; Grunfeld, F.; Unwin, P. R. *Langmuir* **2004**, *20*, 701–707.
- Liu, B.; Rotenberg, S. A.; Mirkin, M. V. *Proc. Natl. Acad. Sci. U.S.A.* **2000**, *97*, 9855–9860.
- Liu, B.; Cheng, W.; Rotenberg, S. A.; Mirkin, M. V. *J. Electroanal. Chem.* **2001**, *500*, 590–597.
- Cai, C.; Liu, B.; Mirkin, M. V.; Frank, H. A.; Rusling, J. F. *Anal. Chem.* **2002**, *74*, 114–119.
- Liu, B.; Rotenberg, S. A.; Mirkin, M. V. *Anal. Chem.* **2002**, *74*, 6340–6348.
- Feng, W.; Rotenberg, S. A.; Mirkin, M. V. *Anal. Chem.* **2003**, *75*, 4148–4154.
- Sun, P.; Laforge, F. O.; Abeyweera, T. P.; Rotenberg, S. A.; Carpino, J.; Mirkin, M. V. *Proc. Natl. Acad. Sci. U.S.A.* **2008**, *105*, 443–448.
- Hengstenberg, A.; Blochl, A.; Dietzel, I. D.; Schuhmann, W. *Angew. Chem., Int. Ed.* **2001**, *40*, 905–908.
- Kurulugama, R. T.; Wipf, D. O.; Takacs, S. A.; Pongmayteegul, S.; Garris, P. A.; Baur, J. E. *Anal. Chem.* **2005**, *77*, 1111–1117.
- Isik, S.; Schuhmann, W. *Angew. Chem., Int. Ed.* **2006**, *45*, 7451–7454.
- Takahashi, Y.; Miyamoto, T.; Shiku, H.; Asano, R.; Yasukawa, T.; Kumagai, I.; Matsue, T. *Anal. Chem.* **2009**, *81*, 2785–2790.

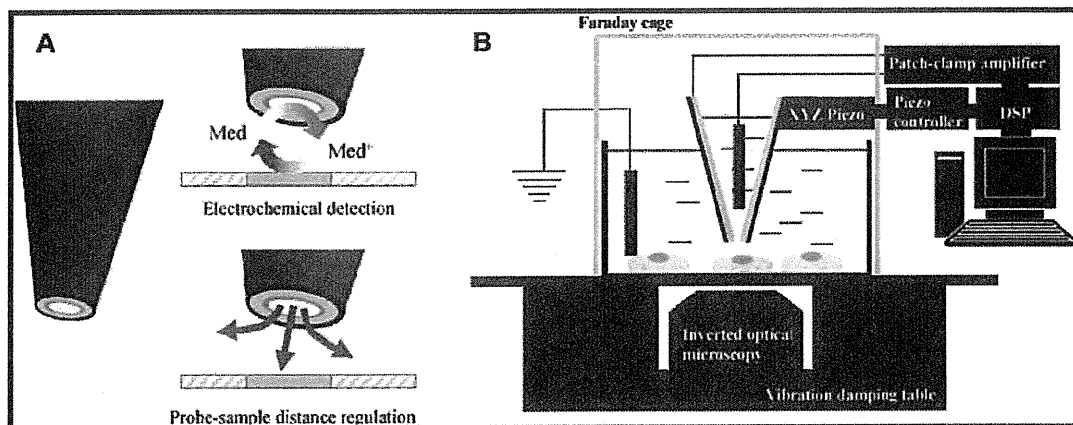


Figure 1. (A) Schematic illustration of the SECM/SICM system probe and (B) the SECM/SICM setup.

Significant efforts have been made to bring the electrode proximate with the sample surface using AFM,^{23–26} shear force,^{8,19,27} and impedance.²⁰ An electrode-patterned cantilever for the AFM/SECM system was fabricated and applied to simultaneous measurements. Carbon nanotube,²⁴ high resistive polymer,²⁵ and nanofabrication technique²⁶ have been adapted for making high aspect ratio shape probes. Nevertheless, it was difficult to apply the system to the measurement of soft samples because the force interaction was usually very unstable to serve as a feedback signal. The degradation of the electrochemical sensitivity caused by undesired electrochemical reactions at the side surfaces of the cantilever is also a problem. Shear force feedback regulation has also been used for control of the probe electrode sample distance. Previously, we reported the simultaneous imaging of the topography and electrochemical signals of single living cells using shear force distance regulation of a ring-type nanoelectrode probe.²⁷ However, preventing probe–cell contact was still difficult because the solution viscosity interfered with the shear force detection. Impedance-based probe–sample distance regulation has been used as a feedback mechanism for noncontact living cell imaging; however, it is difficult to improve the resolution of topography imaging because miniaturization of the electrode degrades the resistance signals for regulating the probe–sample distance.

Scanning ion conductance microscopy (SICM) uses a nanopipette as a scanning probe and provides living cell surface topography images under physiological conditions without physical contact.²⁸ Recent advances in SICM resulted in the development of a novel hopping probe ion conductance microscopy (HPICM) that allows topographical imaging of most convoluted surfaces.²⁹ SICM is based on the phenomenon that the ion flow through a sharp fluid-filled nanopipette is partially occluded when the nanopipette approaches the surface of a sample. Living cell surface topography and dynamic measurements have been performed. Topographical information of the live cell surface can be used to improve the resolution of other analytical tools; SICM nanopositioning system was combined with near field scanning optical microscopy,³⁰ confocal microscopy,³¹ and patch clamps.^{32,33} The nanopipette not only can detect localized ions but can also provide specific ion and biomolecules in a localized place.³⁴

Hersam and co-workers reported combining SECM and SICM and demonstrated simultaneous submicrometer resolution topography and electrochemical imaging of gold film electrodes.³⁵ They used atomic layer deposition (ALD) of aluminum oxide to

conformally insulate a gold-coated nanopipette and focused ion beam (FIB) milling to precisely expose the electrode surface. Bard et al. reported a similar probe design to dispense small amounts of a solution while monitoring the electrochemical response.³⁶

In this work, we demonstrate a hybrid system of SECM and HPICM for simultaneous imaging of topography and electrochemical signal. This system is particularly suitable for detailed characterization of soft biomaterials with complex 3D structures, such as live cells. Figure 1 shows the structure of a nanopipette/nanoring electrode probe and a schematic diagram of the SECM/SICM measurement setup. Ion current flowing between Ag/AgCl electrodes located inside the nanopipette and the outside solution was used as the feedback signal for distance control. The electrochemical signal was acquired with the nanoring electrode. The present study demonstrates that the SECM/SICM system can generate submicrometer resolution images based on topography and electrochemical signals of enzymes on solid surfaces and convoluted living cells. The system was also found to be applicable

- (23) Macpherson, J. V.; Unwin, P. R.; Hillier, A. C.; Bard, A. J. *J. Am. Chem. Soc.* **1996**, *118*, 6445–6452.
- (24) Burt, D. P.; Wilson, N. R.; Weaver, J. M. R.; Dobson, P. S.; Macpherson, J. V. *Nano Lett.* **2005**, *5*, 639–643.
- (25) Patil, A.; Sippel, J.; Martin, G. W.; Rinzler, A. G. *Nano Lett.* **2004**, *4*, 303–308.
- (26) Shin, H.; Hesketh, P. J.; Mizaiakoff, B.; Kranz, C. *Anal. Chem.* **2007**, *79*, 4769–4777.
- (27) Takahashi, Y.; Shiku, H.; Murata, T.; Yasukawa, T.; Matsue, T. *Anal. Chem.* **2009**, *81*, 9674–9681.
- (28) Korchev, Y. E.; Bashford, C. L.; Milovanovic, M.; Vodyanoy, I.; Lab, M. J. *Biophys. J.* **1997**, *73*, 653–658.
- (29) Novak, P.; Li, C.; Shevchuk, A. I.; Stepanyan, R.; Caldwell, M.; Hughes, S.; Smart, T. G.; Gorelik, J.; Ostanin, V. P.; Lab, M. J.; Moss, G. W.; Frolenkov, G. I.; Klenerman, D.; Korchev, Y. E. *Nat. Methods* **2009**, *6*, 279–281.
- (30) Korchev, Y. E.; Raval, M.; Lab, M. J.; Gorelik, J.; Edwards, C. R. W.; Rayment, T.; Klenerman, D. *Biophys. J.* **2000**, *78*, 2675–2679.
- (31) Gorelik, J.; Shevchuk, A.; Ramalho, M.; Elliott, M.; Lei, C.; Higgins, C. F.; Lab, M. J.; Klenerman, D.; Krauszewicz, N.; Korchev, Y. *Proc. Natl. Acad. Sci. U.S.A.* **2002**, *99*, 16018–16023.
- (32) Korchev, Y. E.; Negulyaev, Y. A.; Edwards, C. R. W.; Vodyanoy, I.; Lab, M. J. *Nat. Cell Biol.* **2000**, *2*, 616–619.
- (33) Gorelik, J.; Gu, Y. C.; Spohr, H. A.; Shevchuk, A. I.; Lab, M. J.; Harding, S. E.; Edwards, C. R. W.; Whitaker, M.; Moss, G. W. J.; Benton, D. C. H.; Sanchez, D.; Darszon, A.; Vodyanoy, I.; Klenerman, D.; Korchev, Y. E. *Biophys. J.* **2002**, *83*, 3296–3303.
- (34) Piper, J. D.; Li, C.; Lo, C. J.; Berry, R.; Korchev, Y.; Ying, L. M.; Klenerman, D. *J. Am. Chem. Soc.* **2008**, *130*, 10386–10393.
- (35) Comstock, D. J.; Elam, J. W.; Pellin, M. J.; Hersam, M. C. *Anal. Chem.* **2010**, *82*, 1270–1276.
- (36) Walsh, D. A.; Fernandez, J. L.; Mauzeroll, J.; Bard, A. J. *Anal. Chem.* **2005**, *77*, 5182–5188.

for evaluating the permeation property of electroactive species through cellular membranes. To our knowledge, this is the first report of high-resolution imaging of biomaterials with SECM/SICM.

Material and Methods

Reagents. Glucose oxidase (GOD; Biozyme Laboratories), horse radish peroxidase (HRP; Wako), L-15 medium (Gibco, Parsiply, UK), ferrocenylmethanol (FcCH₂OH; Aldrich), potassium hexacyanoferrate (II) trihydrate (K₄Fe(CN)₆·3H₂O; Kanto chemical Co., Inc.), glutaraldehyde (GA; Wako), and bovine serum albumin (BSA; Wako) were purchased and used as received. PBS was prepared from 7.2 mM Na₂HPO₄ 12H₂O, 2.8 mM KH₂PO₄, and 150 mM NaCl (pH 7.0).

Fabrication of the SECM/SICM Electrode. A glass capillary (World precision Instruments, Inc., PG10165-4) was pulled using a capillary puller (Narishige PE-21). This capillary was then coated by Ti/Pt or Ti/Au sputtering (Anelva, L-332S-FH, RF200), followed by insulation with an anodic electrophoretic paint (Elecoat AE-X, Shimizu Co., Ltd.) by immersing the top of the metal-coated capillary and applying a DC potential of +2.0 V for 2 min between the capillary and counter electrode. After electrophoretic deposition, the electrode was removed from the solution, washed for 10 s to remove excess paint solution, and cured in an oven for 45 min at 150 °C to harden the insulation layer. To expose an electroactive area and form an ion transport aperture, the probe apex was milled by a focused ion beam (FIB, Seiko Instruments, SMI 2050).

Preparation of the Enzyme Spot. A PBS solution containing 1 mg/mL enzyme, 5 mg/mL BSA, and 1% GA was spotted on an APS-coated glass slide (Matsunami Glass Ind., Ltd.) and dried in air for 30 min.

Cell Culture and Isolation. A single A6 cell line was kindly provided by Dr. P. DeSmet (Karnolieke Universiteit, Belgium). All experiments were performed between 127 and 134 passages. Cells were cultured, as described previously.³⁷

Superior cervical ganglion (SCG) cells were kindly provided by Dr. Guy Moss. Cells were cultured at a high density (9×10^5 cells/mL) on poly-L-lysine-coated coverslips. Cells were kept in a growth medium consisting of a DMEM (Gibco) supplemented with 10% fetal bovine serum (Gibco), 100 µg/mL streptomycin and 100 U/mL penicillin (Gibco), nerve growth factor (67 ng/mL, 2.5 S; Gibco). Cells were maintained at 37 °C in an atmosphere of humidified air with 95% O₂/5% CO₂. Cells were used for SECM/SICM measurements after 2–5 days when they had migrated to form cell clusters connected by axon bundles.

Cardiac myocytes from adult rats were isolated by digestion of intact perfused ventricle, according to the method previously described.³⁸

Instrumentation. Figure 1B shows a schematic diagram of the SECM/SICM instrument, which has been previously described.³² The currents were measured with a dual channel MultiClamp700B patch-clamp amplifier (Axon Instruments). The electrochemical and ion current signals were low-pass filtered at 40 Hz and 1 kHz, respectively. The data was digitized and analyzed with continuous data acquisition hardware and software (Axon Digidata 1322A, Axon Instruments). The probe position was controlled by a XY and Z piezoelectric scanner (Physik Instrumente, 621.2CL and 621.ZCL), which was controlled with an amplifier module (Physik Instrumente, E-503.00) and servo control module (Physik Instrumente, E-509.C3). The system was controlled by a program written with Delphi (Borland) and Code Composer Studio (Texas Instruments, U.S.A.) for ScanIC controller (Ionscope, UK).

SECM/SICM Measurements. The nanopipette electrode brought near the sample surface used ion current as the feedback signal and acquired height information. The electrochemical measurement was performed by the nanoring electrode. A hopping mode²⁹ was adopted as the scanning method. Briefly, the vertical Z positioning of the hopping probe and the movement of the sample in the XY plane were controlled at a sampling frequency of 20 kHz. A five-step procedure was used to determine the height and detect electrochemical species of the specimen at each imaging point. First, the probe was withdrawn a specified distance from its existing position. Second, the vertical position of the probe was maintained for 10 ms, while the nanopositioning stage moved to a new imaging point in the XY plane. During this time a reference current, I_{REF} , was measured as an average of the DC current through the probe. Third, the probe was lowered at constant fall rate of 15 nm/ms while monitoring the difference in the current, I , between I_{REF} and the instantaneous current through the probe I_{MV} . As soon as I drop exceeded the specified value of the set point, I_S , which was approximately 1.0–1.5% of I_{REF} , the vertical position of the probe was saved into the corresponding image pixel. Fourth, electrochemical measurement was performed for 200 µs using the nanoring electrode. Finally, the probe was quickly withdrawn by a specified hop amplitude to start a new measurement cycle.

Results and Discussion

Characterization of the SECM/SICM Probe. Panels A and B of Figure 2 show the SEM images and the structure of the SECM/SICM probe apex, respectively. The nanopipette aperture radius was found to be 220 nm. The Au nanoring electrode for SECM measurements was fabricated outside of the glass sheath, and the inner and outer radii of the nanoring electrode were found to be 330 and 550 nm, respectively. The SECM nanoring electrode was coated with a 70 nm thick insulator film. The probe angle was less than 10°, which allowed the probe to access a relatively high aspect sample. Figure 2C shows a cyclic voltammogram (CV) of 0.50 mM ferrocenylmethanol (FcCH₂OH), observed on the SECM nanoring electrode in 0.1 M KCl at a scanning rate of 100 mV/s. The voltammogram shows a sigmoidal shape with the steady-state current of 500 pA, which is approximately 6 times larger than that expected for a microdisk electrode with the same electrode size. The larger current is probably due to defects in the insulating layer. The defects did not cause a serious problem in SECM imaging based on generation collection (GC) and feedback (FB) measurements, as shown later. The SECM/SICM probe with a SECM Pt nanoring electrode also showed similar electrochemical behavior. Since the Pt nanoring electrode showed undesirable electrochemical responses in H₂O₂ solution, the probe with an Au nanoring electrode was used for imaging in H₂O₂ solutions, as described later.

Figure 3 shows approach curves to conductive and insulating substrates. The potentials of the SECM Pt and SICM Ag/AgCl electrodes were set at 500 and 200 mV, respectively. In either case, the ion current signal decreased as the tip approached the sample surface ($z \rightarrow 0$), which illustrates the fundamental nature of the ion current, blocked by either electron-insulating or electron-conducting surfaces. The distance for a 1% change of the SICM response (ion current) was almost the same as the nanopipette inner radius, in this case 220 nm. The experimental results were in good agreement with theory classified in reference 28. On the other hand, the approach curves of the electrochemical current signal for the insulating and conducting substrates showed negative and positive feedback features, respectively. The change in the electrochemical current was small probably due to the electrochemical reaction through the defects of the probe insulating wall. Importantly, no interference

(37) Gorelik, J.; Shevchuk, A. I.; Frolenkov, G. I.; Diakonov, I. A.; Lab, M. J.; Kros, C. J.; Richardson, G. P.; Vodyanov, I.; Edwards, C. R. W.; Klenerman, D.; Korchev, Y. E. *Proc. Natl. Acad. Sci. U.S.A.* **2003**, *100*, 5819–5822.

(38) Lyon, A. R.; MacLeod, K. T.; Zhang, Y.; Garcia, E.; Kanda, G. K.; Lab, M. J.; Korchev, Y. E.; Harding, S. E.; Gorelik, J. *Proc. Natl. Acad. Sci. U.S.A.* **2009**, *106*, 6854–6859.

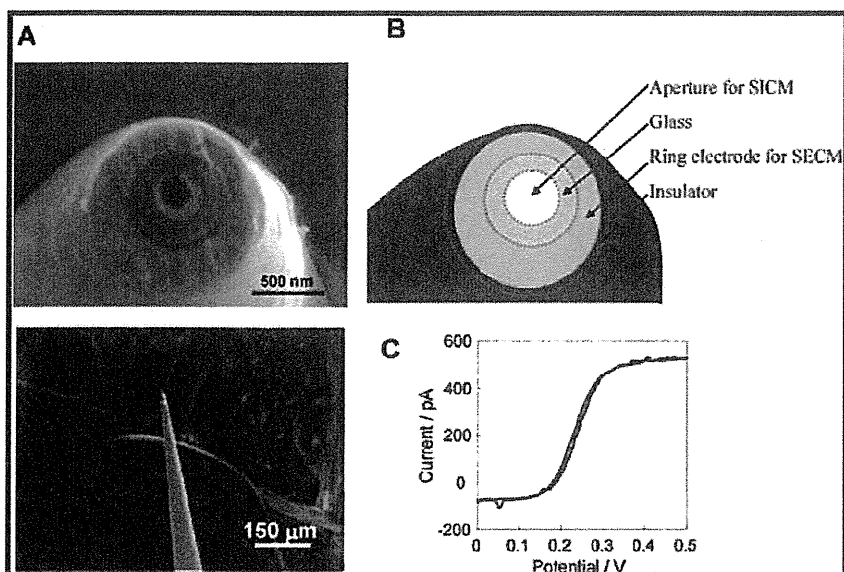


Figure 2. (A) SEM micrographs of the SECM/SICM probe. (B) Schematic illustration of probe structure. (C) Cyclic voltammogram of 0.50 mM FcCH_2OH on a SECM nanoring electrode in a 0.1 M KCl solution at a scanning rate of 100 mV/s. The nanopipette aperture radius was 220 nm. Inner and outer radii of the SECM Au nanoring electrode were 330 and 550 nm, respectively. The insulator was 70 nm thick.

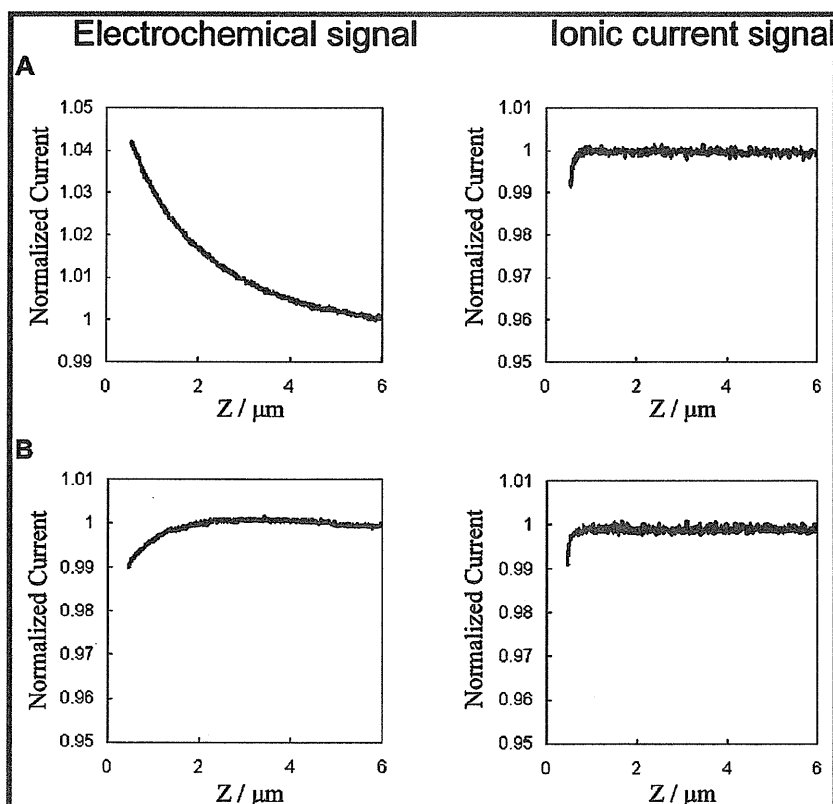


Figure 3. Approach curves of a SECM/SICM electrode to a (A) conductive Pt and (B) insulated glass surface in a 0.50 mM FcCH_2OH + 0.1 M KCl solution for simultaneous electrochemical (left) and ion current (right) measurements. The SECM nanoring and SICM nanopipette electrodes were held at 500 and 300 mV vs Ag/AgCl, respectively.

was observed from CV measurements between the ion and electrochemical currents at the electrodes (Supporting Information, Figure S1). This indicated that interference between the nanoring electrode and Ag/AgCl electrode does not occur in simultaneous topographical and electrochemical imaging.

Imaging a Pt Interdigitated Array Electrode (IDA). We measured a Pt interdigitated array electrode (IDA) to show the noncontact distance regulation of SECM/SICM. If the probe collides with the IDA during scanning, it may break, resulting in an abrupt ion current increase, making it impossible to